SUPPLEMENTAL MATERIALS for

Total angular momentum dichroism of the terahertz vortex beams at the antiferromagnetic resonances

A. A. Sirenko[1,2]*, P. Marsik[2], L. Bugnon[2], M. Soulier[2], C. Bernhard[2], T. N. Stanislavchuk[1], Xianghan Xu[3], and S.-W. Cheong[3]

[1] Department of Physics, New Jersey Institute of Technology, Newark, New Jersey 07102, USA

[2] Department of Physics, University of Fribourg, CH-1700 Fribourg, Switzerland

[3] Rutgers Center for Emergent Materials and Department of Physics and Astronomy, Rutgers University, Piscataway, New Jersey 08854, USA.

* Correspondence and requests for materials should be addressed to A. A. S. (email: sirenko@njit.edu)

1. Experimental setups for the vortex beams

Fig. S1 shows schematics for the axicon-based experimental setup used for the generation of the vortex beams in FIG. 1(c,d) of the manuscript. The setup has been previously described in Ref. [1]. It consists of a linear polarizer, a two-bounce Fresnel prism (FP) made of TOPAS, and a 4-bounce axicon made of transparent silicon. The two-bounce FP served as a broad-band retarder to convert the input linear polarization $(\vec{e}_x \pm \vec{e}_y)$ to the right-hand $\vec{e}_R = \vec{e}_x - i\cdot\vec{e}_y$ or left-hand $\vec{e}_L = \vec{e}_x + i\cdot\vec{e}_y$ circular polarizations. An axicon retarder is a converter between circularly polarized light and vortex beams, or between light with spin angular momentum (SAM) and orbital angular momentum (OAM). It was designed to produce broad-band THz vortex beams with OAM $|l|$=1. The electric field distribution in the output beam is $\vec{e}_l(\vec{r},\phi) \approx (\vec{r}/r)\cdot\exp[i\cdot l\cdot(\phi-\phi_0)]$, where ϕ is the vortex phase, l=+1 or l=–1, the initial phase is $\phi_0 = 3\pi/4$, and $\vec{r}$ is the radial coordinate. The switch between l=+1 and l=–1 outputs is produced by rotation of the linear polarizer at the input of the setup between two orthogonal positions: $(\vec{e}_x + \vec{e}_y)$ and $(\vec{e}_x - \vec{e}_y)$. Calculated radially independent electric fields $\vec{e}_{+1}(\vec{r},\phi)$ and $\vec{e}_{-1}(\vec{r},\phi)$ are also shown in Fig. S1. Note that such beams have a non-zero curl of the electrical

field $\vec{e}_{\pm 1}(\vec{r},\phi)$ around the beam axis $\nabla\times\vec{e}_{\pm 1}(\vec{r},\phi)\neq 0$ that is collinear with the $\vec{k}$ vector of the light. Note here that the circularly polarized light at the input of the axicon cannot "leak" through. First, the axicon uses 4-bounces of the total internal reflections, the same as in a 4-bounce Fresnel prism that is known to be a perfect converter between circular and linear polarizations. Furthermore, because time-domain spectroscopy is used, any "leaking" circularly polarized photons that bypass the axicon or those not experiencing the expected four bounces would arrive at the detector at a completely different time than the major pulse. Thus, the leaking photons cannot contribute to the measured interferogram.

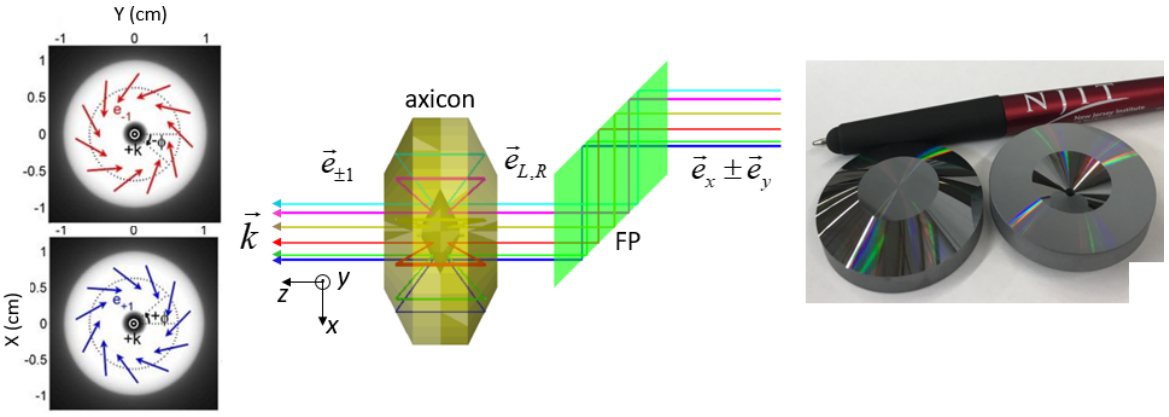

FIG. S1. The central panel shows the conversion of the circularly polarized light into vortex beam modes $\vec{e}_{+1}(\vec{r},\phi)$ and $\vec{e}_{-1}(\vec{r},\phi)$ using a combination of a two-bounce Fresnel prism (FP) and an axicon (adapted from Ref. [1]). After passing through an FP retarder, the linearly polarized light $(\vec{e}_x+\vec{e}_y)$ or $(\vec{e}_x-\vec{e}_y)$ becomes circularly polarized $\vec{e}_L=\vec{e}_x+i\cdot\vec{e}_y$ or $\vec{e}_R=\vec{e}_x-i\cdot\vec{e}_y$. After passing through the axicon, the beam acquires a vortex phase $\vec{e}_{+1}(\vec{r},\phi)$ or $\vec{e}_{-1}(\vec{r},\phi)$ while losing its circular polarization. The electric field distribution is shown in the left panel where the $\vec{k}$ vector is normal to the page. The right panel shows a photo of the axicon retarder.

Fig. S2(a,b) shows schematics for the experimental setups with the spiral plate used for the generation of the Laguerre-Gaussian (LG) vortex beams with $|l|>1$. These setups were used for experimental data in FIG. 2, FIG. 3, and FIG. 4 of the manuscript. To obtain an OAM with $|l|>1$, the broadband axicon was replaced with pairs of two identical 3D-printed transparent spiral plates. The spiral plates were produced with a Formlabs Form2 3D printer using clear V4 resin. In FIG. S2(a) the polarization input is linear $\vec{e}_y$ that produced the OAM at the sample position with the field distribution of $\vec{e}_l(\phi)\approx\vec{e}_y\cdot\exp[i\cdot l\cdot\phi]$, where l takes integer values of $l=\pm 2,\pm 3,$

or ±4 at the corresponding frequencies ν_l. The field distribution across the beam at the sample position is shown in the right panel. Note that the first spiral plate created the vortex beam at the sample, while the second plate unwound the vortex wave front such that a plane wave propagates further to the detector. The handedness of the 3D printed spirals determines the sign of *l*. Several frequencies ν_l with integer values of *l*'s were simultaneously present in the measured spectra *I*(ν). The integer value of *l* at a given frequency ν_l (or wavelength λ_l) is determined by the step height *h* and the refractive index *n*=1.56 of the spiral plate: $l \cdot \lambda_l = h(n-1)$ [2]. FIG. S2(b) shows the same setup but with a circularly polarized input polarization. Such THz beams have a combined total angular momentum (AM) of $j = l + \sigma$ with σ = ±1 and integer values of $l = \pm 2, \pm 3,$ or ±4 and the field distribution $\vec{e}_j(\phi) \approx \vec{e}_{L,R} \cdot \exp[i \cdot l \cdot \phi]$ across the LG vortex beams. Both beams shown in FIG.S2(a,b) have a constant field across the beam with no curl: $\nabla \times \vec{e}_y = 0$ and $\nabla \times \vec{e}_{R,L} = 0$.

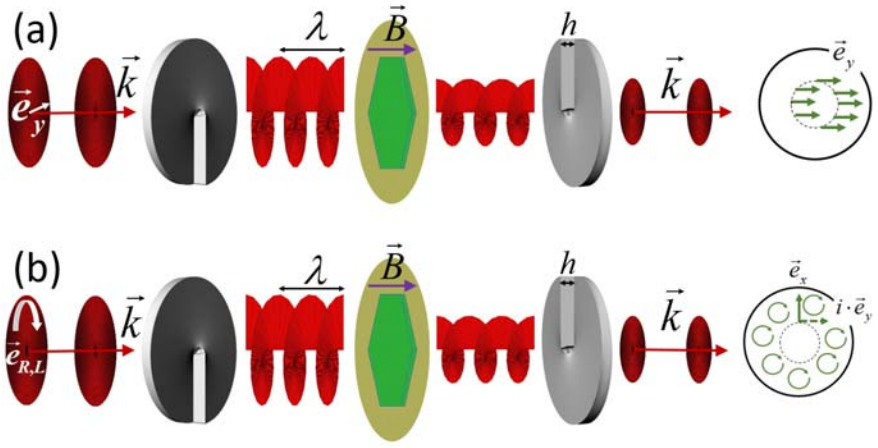

FIG. S2 (a) Schematics for the measurement geometry with a linear polarization $\vec{e}_y$ for the THz beam input. (b) The same with a circular polarization $\vec{e}_{R,L}$ for the THz beam input. Sample (green hexagon) is placed between a pair of identical spiral plates with step height *h*.

2. Experimental characterization of the THz vortex beams

For experimental characterization of the THz vortex beams produced with the 3D printed spiral plates we used the same experimental setup as for the sample measurements. We mounted an empty metal aperture at the sample position on an XY motorized translational stage. The

distance between the aperture and the spiral plate was 11 cm. The optical setup consisted of a rotatable linear polarizer, a Fresnel two-bounce prism, a vortex plate that produced OAM of l=2 at the light frequency of 0.5 THz (λ= 0.6 mm), and an aperture (see FIG. S3). The beam footprint at the sample position has the measured full width at half maximum (FWHM) of about 9 mm. The aperture diameter was chosen to be 2 mm, which allowed us to keep the transmitted signal at a high signal-to-noise ratio. The cross section of the beam was scanned with the steps Δx and Δy of 1 mm, or half the aperture diameter. This beam characterization has two goals: (i) to demonstrate the expected toroidal intensity shape and the phase variation around the beam, and (ii) to demonstrate that the linear and circular polarizations of the photons remains nearly unchanged after passing through the spiral plate. In the following we will demonstrate that the vortex beams have the expected shape and phase, and they can also carry spin angular momenta, also known as right- and left-hand circular polarizations.

FIG. S4 shows a map for the beam amplitude, two cross sections along X and Y directions and an integrated radial distribution of the amplitude. The input linear polarizer is at zero angle P with respect to the *y*-axis (see FIG.S1 for x-y-z notation), producing $\vec{e}_y$. After passing through the Fresnel prism, the beam polarization does not change. As expected, the beam has a toroidal shape with the Amplitude minimum close to the center. The outside dimensions of the beam with FWHM of about 8 mm are determined by the focusing optics for the original Gaussian beam produced by the 50 mm-diameter parabolic mirror with the apparent focus distance of 500 mm. The measured amplitude in the very center of the beam is at 20% of the maximum that is very

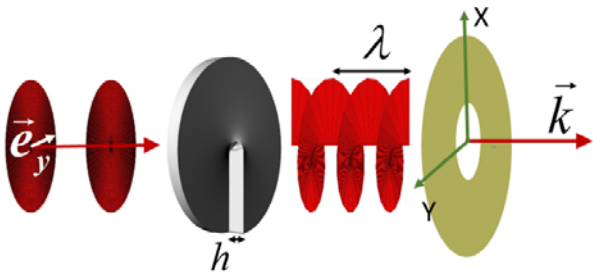

FIG.S3. Schematics of the experimental setup for the vortex beam characterization. The aperture diameter is 2 mm, the distance between the spiral plate and the aperture is 11 cm. The input linear polarization $\vec{e}_y$ (or circular polarizations $\vec{e}_R = \vec{e}_x - i \cdot \vec{e}_y$ and $\vec{e}_L = \vec{e}_x + i \cdot \vec{e}_y$) are produced with a combination of a linear polarizer and a Fresnel prism.

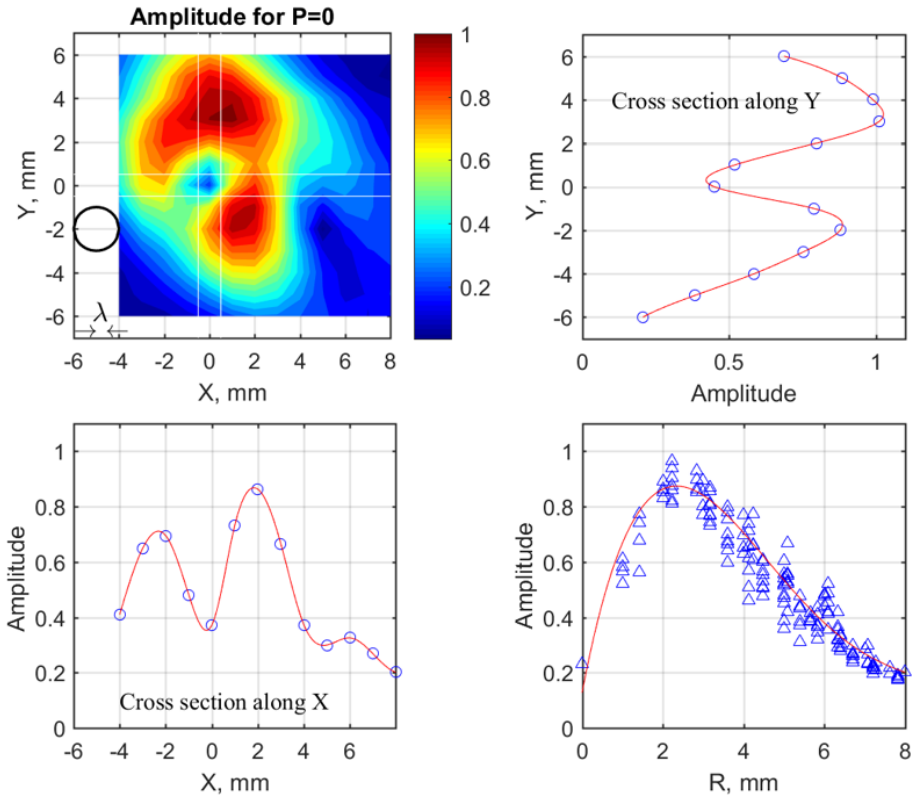

FIG.S4. The normalized 12 mm × 12 mm map of the signal Amplitude at 0.5 THz for the input linear polarization with P = 0 ($\vec{e}_y$). Black circle shows the aperture size; the wavelength is shown with two black arrows. The side panels present the amplitude cross sections along the bands shown with white lines. The radial dependence of the signal amplitude shows the intensity peak at about 3 mm with respect to the center of the beam and a minimum of amplitude at the center. Red curves guide the eye.

reasonable for the measurement with an aperture whose dimensions are close to the diffraction limit. Note that the same diffraction effect results in the beam broadening at the sample position. In the actual experiments we estimated the FWHM of the unrestricted beam to be closer to 7 mm at the sample. By rotating the input linear polarizer *P* to +45° or +315° (=-45°) , we produced one of the two circular polarizations at the vortex spiral plate with $\vec{e}_R = \vec{e}_x - i \cdot \vec{e}_y$ or $\vec{e}_L = \vec{e}_x + i \cdot \vec{e}_y$, respectively. Still, the corresponding intensity maps did not change significantly and they are very similar to that in FIG. S4. The Amplitude maps and cross sections for *P* = +45° and +315° are shown in FIG. 5.

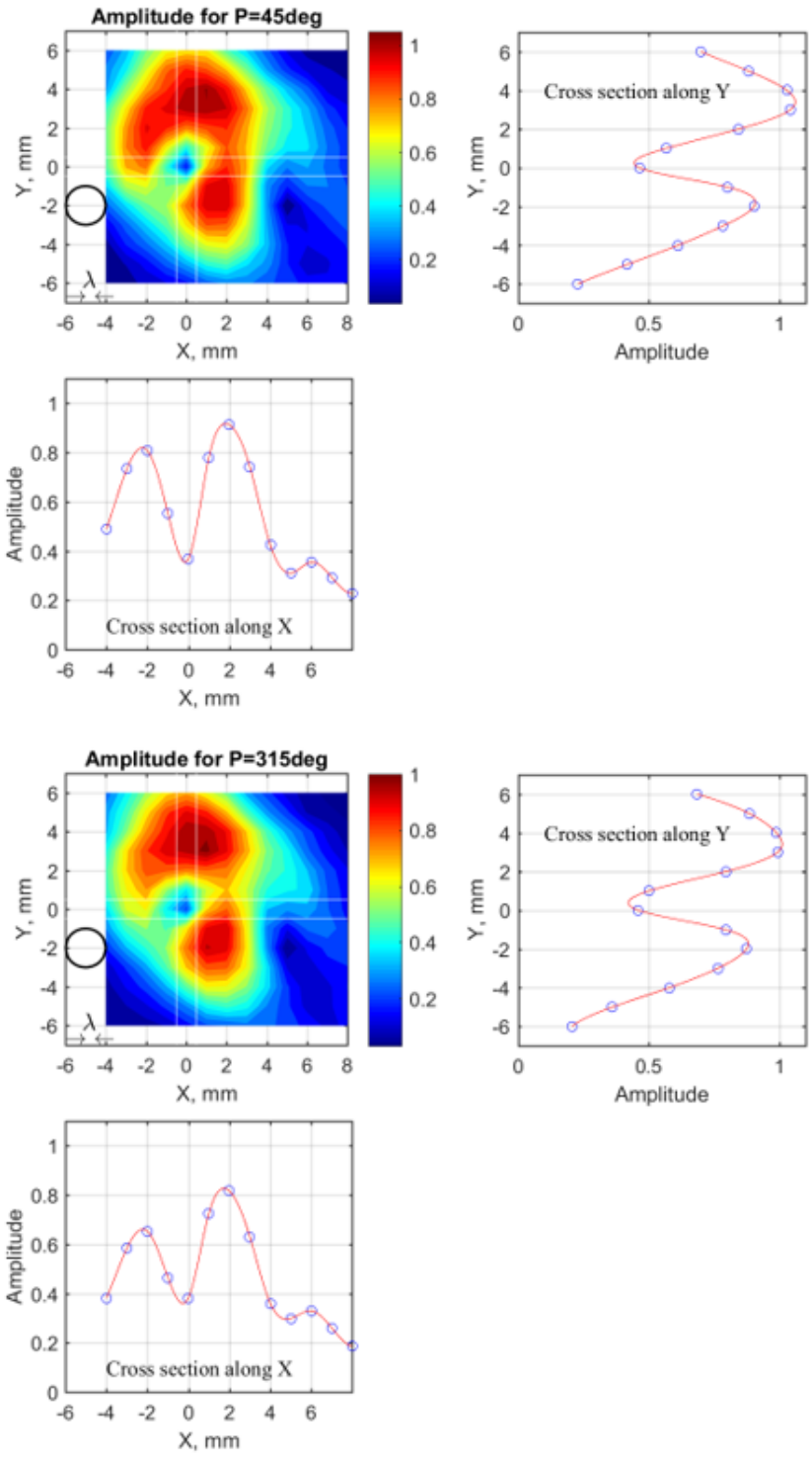

FIG.S5. The same as in FIG. S4 for the two circularly polarized inputs with P = 45° (top) and P = 315° (bottom).

FIG. S6 shows phase maps measured for three input linear polarizations P=0, +45°, and +315°. In addition, the same Figure shows azimuthal variation of the map for 360 degrees around the beam propagation direction at R=3 mm. As expected, the phase for the beam produced with a spiral plate with l=2 changes by $2\pi l$ for 360° rotation around the beam direction. The bottom panels show the experimental points from the map and red solid lines for theoretical expectation for the beam phase. Two very similar dependencies for the phase variation were measured for

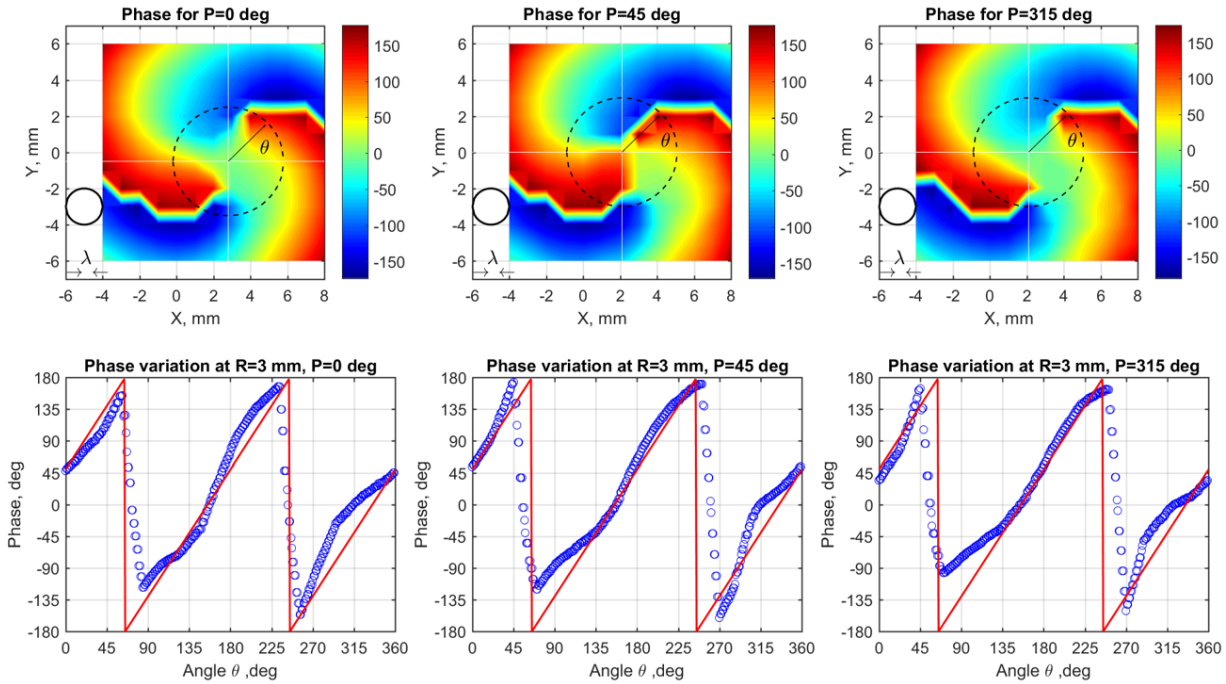

FIG.S6. The signal phase at 0.5 THz for the input linear polarization with P = 0 (left), P = 45° (center), and P = 315° (right). (Black circle shows the aperture size; the wavelength is shown with two black arrows. The bottom panels present the azimuthal dependence of the phase extracted from the map along the black dotted circle with R=3 mm. Red lines show theoretical dependence of the phase that changes by 4π for the vortex plate with l=2 at 0.5 THz.

P=+45°, and +315° as well (see FIG. S6).

Let's turn our attention to the polarization properties of the individualrays composing the vortex beams. In the first approximation, the polarization state of individualrays passing through the spiral plate should be the same as created by the combination of the linear polarizer and the

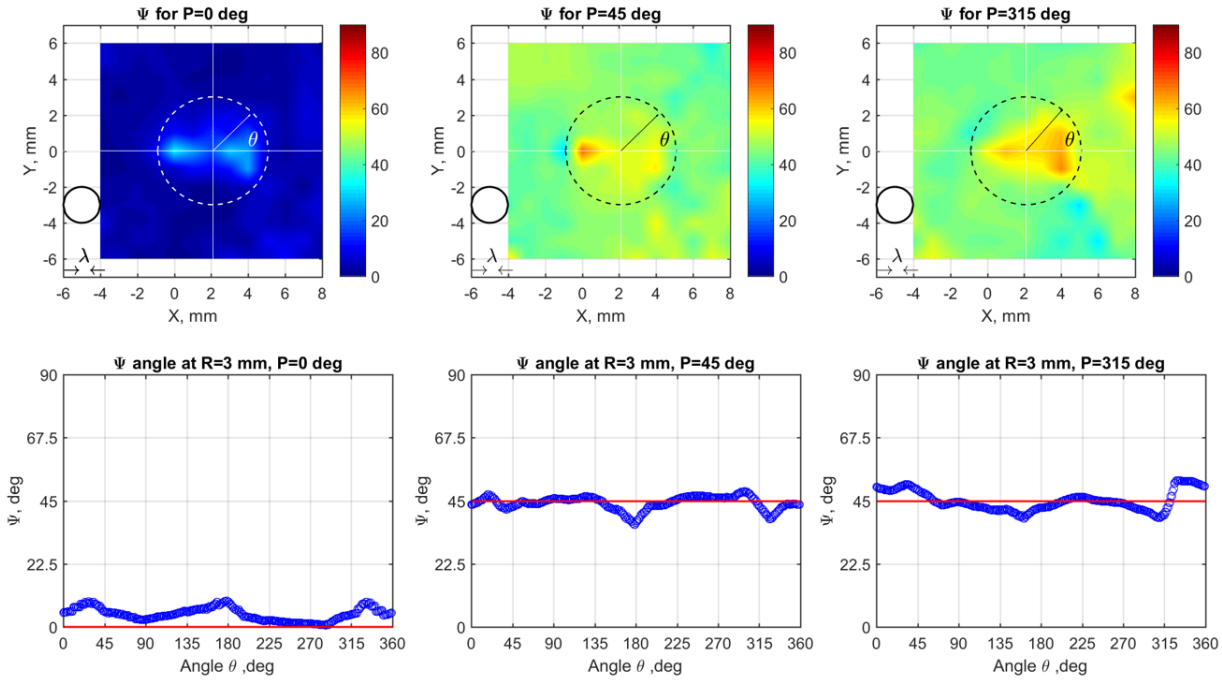

FIG.S7. The polarization angles Ψ at 0.5 THz for the input linear polarization with P = 0 (left), P = 45° (center), and P = 315° (right). The bottom panels present the azimuthal dependence of the Ψ values extracted from the map along the black dotted circle with R=3 mm. Red lines show theoretical value of Ψ being 0 for linear polarization and 45° for both circular polarizations.

Fresnel prism. The only deviations from that could have been produced by imperfections of the spiral plates, that however were printed in a solid form with 0.025 mm resolution that is ~ 25 times better than the wavelength λ= 0.6 mm. For experimental characterization of the beam polarization we used the conventional rotating analyzer method [3]. The experimental results are presented below using the following Jones vector conventions. The ratio of the electric field amplitudes $\left|\vec{e}_x / \vec{e}_y\right| = \tan\Psi$ and the phase difference between the two complex vectors $\vec{e}_y$ and $\vec{e}_x$ is Δ. In this notation, light with linear polarization along *y*, should have $\Psi = 0$ and undefined Δ. For two circular polarizations, $\vec{e}_L = \vec{e}_x + i\cdot\vec{e}_y$ and $\vec{e}_R = \vec{e}_x - i\cdot\vec{e}_y$, the following values are expected: $\Psi = 45°$ and $\Delta = \pm 90°$.

FIG. S7 and FIG. 8 show experimental maps for Ψ and Δ, correspondingly, measured for *P*=0, +45°, and +315°. The azimuthal variations are shown with blue symbols along with the

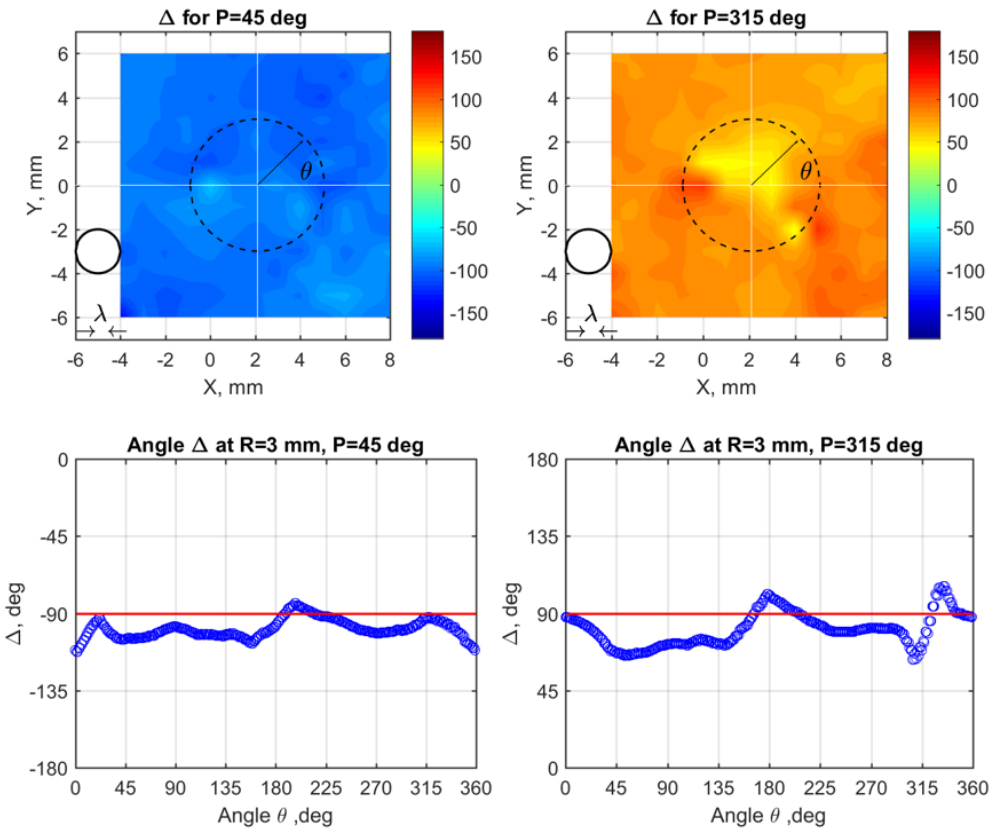

FIG.S8. The polarization angles Δ at 0.5 THz for inputs with two circular polarizations with P = 45° (left) and P = 315° (right). The bottom panels present the azimuthal dependence of the Δ values extracted from the map along the black dotted circle with R=3 mm. Red lines show the theoretical value of Δ being +90° and -90° for two circular polarizations. Note that Δ is undefined for the linear polarization input with P = 0 and, thus, it is not shown here.

corresponding theoretical expectations shown with horizontal red lines. The close proximity between the experiment and theory provides a proof that the THz vortex beams used in our experiments possess simultaneously the vortex phase, which is the property of the beam, and the spin angular momentum $\sigma = \pm 1$ for the corresponding input circular polarizations and $\sigma = 0$ for the input with a linear polarization. Our results for intensity maps are similar to that previously reported for 3D spiral plates used to produce THz vortex beams [4]. Note that the minor deviation of our experimental data from the theory may be primarily due to the small aperture diameter of 2 mm that brings the beam mapping close to the diffraction limit for λ= 0.6 mm. We

believe that the unrestricted vortex beams are closer to the theoretical expectation than the mapping results that are presented here.

[1] A. A. Sirenko, P. Marsik, C. Bernhard, T. N. Stanislavchuk, V. Kiryukhin, and S-W. Cheong, Phys. Rev. Lett. **122**, 237401 (2019).
[2] J. Sun, J. Zeng, X. Wang, A. N. Cartwright, and N. M. Litchinitser, Scientific Reports **4**, 4093 (2014).
[3] P. Marsik, K. Sen, J. Khmaladze, M. Yazdi-Rizi, B. P. P.Mallett, and C. Bernhard, Appl. Phys. Lett. **108**, 052901 (2016).
[4] Changming Liu, Jinsong Liu, Liting Niu, Xuli Wei, Kejia Wang, and Zhengang Yang Scientific Reports **7**, 3891 (2017).